Journal of Applied Polymer Science

Synthesis of iron oxides intercalated montmorillonite and α-zirconium phosphate particles and their applications in polystyrene composites

Xiaofang Tan,[1] Hongdian Lu,[1] Juan Wang,[1] Chen Jin,[2] Wei Yang,[1] Quanzheng Zhang[1]

[1]Department of Chemical and Materials Engineering, Hefei University, Hefei, Anhui 230601, People's Republic of China

[2]Department of Waste Management, Institute of Environmental Engineering, Faculty of Agricultural and Environmental Sciences, University of Rostock, Rostock 18509, Germany

Correspondence to: H. Lu (E-mail: hdlu@ustc.edu.cn)

ABSTRACT: Three kinds of particles of organically modified montmorillonite (OMT) intercalated with iron oxides (Fe-OMT), hexadecyltrimethylammonium bromide (CTAB) and ethylamine (EA)-modified zirconium phosphate (ZrP) intercalated with iron oxides, named as Fe-ZrP(CTAB) and Fe-ZrP(EA), respectively, were synthesized through a simple route. Characterization of these particles showed that they had a mesoporous lamellar structure with high specific surface area and mesoporous volume. The influence of these particles on the thermal properties and combustion effluents of polystyrene (PS) were comparatively studied with the widely used OMT. The results suggested that the presence of Fe-OMT, Fe-ZrP(CTAB), and Fe-ZrP(EA) imparted PS with an increased thermal degradation onset temperature and a higher glass transition temperature, but they could not increase the thermo-oxidative stability remarkably as OMT did. Meanwhile, Fe-ZrP(CTAB) and Fe-ZrP(EA) exhibited stronger acidity and higher efficiency in preventing the condensed phase oxidation than either OMT or Fe-OMT, since they imparted the PS composites with a higher ratio of CO/CO_2 in the combustion effluents. © 2015 Wiley Periodicals, Inc. J. Appl. Polym. Sci. **2015**, *132*, 42737.

KEYWORDS: composites; polystyrene; thermal properties

Received 1 December 2014; accepted 16 July 2015

DOI: 10.1002/app.42737

INTRODUCTION

Thermoplastics such as polystyrene (PS), poly (methyl methacrylate) (PMMA), and polypropylene (PP) are widely used in household appliances and packaging containers and so on. Thus, the improvement in thermal stability and flammability performance of these polymeric materials is a major concern in industries.

For the past decades, layered compounds mainly organically modified montmorillonite clay (OMT), which possess high aspect ratio and can be nano-dispersed throughout polymeric matrix, have been intensively studied to improve the thermal stability and flame retardancy of PS, PMMA, and PP by fabricating polymer-clay nanocomposites; it is believed that the improvement is mainly derived from the barrier effect caused by the reassembly of nano-dispersed clay layers on the surface that prevents the transfer of mass and heat.[1–4] Besides OMT, α-zirconium phosphate (ZrP) having OMT-like lamellar structure is another kind of emerging particles for improving polymeric materials properties.[5,6]

The use of transition metal oxides such as manganese oxide (MnO_2), titanium oxide (TiO_2), and iron oxide (Fe_2O_3) alone or as synergistic agents in addition to layered compounds and traditional flame retardants to improve polymeric materials thermal stability and flame retardancy has attracted much interest.[7–9] For example, Ferriol group had studied the thermal properties of PMMA with metal oxides alone, and PMMA with the combination of metal oxides and OMT; it was found that the thermal stability of PMMA was improved significantly.[10,11] On the contrary, thermal degradation of PS and PP can be catalyzed by the incorporation of transition metal oxides at relative low temperature range 250–500°C, due to transition metal oxides can catalyze the formation of macroradical through random and chain end scissions.[12,13] It therefore seems that transition metal oxides have different effects on various polymer degradations, retarding or catalyzing the thermal degradation processes. Moreover, when some transition metal oxides, such as MnO_2 and copper oxide (CuO), were introduced in the interlay spaces of OMT, the pillared materials showed potential solid acid catalytic effect on the combustion of volatile organic compounds (VOCs).[14,15]

In order to understand how the transition metal oxides modified layered compounds influence the thermal properties and combustion effluents of polymer composites, three kinds of iron

Table I. TGA Data, T_g and CO/CO_2 Ratios of Polystyrene Composites

	In a nitrogen atmosphere				In an air atmosphere					
Sample	$T_{5\%}$ (°C)	$T_{50\%}$ (°C)	T_{max} (°C)	Char (%, 500°C)	$T_{5\%}$ (°C)	$T_{50\%}$ (°C)	T_{max} (°C)	Char (%, 500°C)	T_g (°C)	CO/CO_2 (ppm/ppm)
PS/SMA	372	412	420	0.7	319	378	391	2.1	98.6	0.179
PS/SMA/OMT(10%)	370	425	435	6.3	334	407	425	8.2	103.2	0.184
PS/SMA/Fe-OMT(10%)	382	421	423	10.2	317	397	408	11.2	104.6	0.188
PS/SMA/Fe-ZrP(EA) (10%)	372	421	425	10.2	331	400	410	10.8	103.5	0.230
PS/SMA/Fe-ZrP(CTAB) (10%)	376	420	424	10.8	312	382	399	11.9	104.6	0.194

oxides intercalated layered compounds including OMT and ZrP particles were prepared through a facile way using iron benzoate complex as precursor. PS composites with these particles were then prepared by melt blending. The differences in the thermal properties and the ratio of CO/CO_2 in combustion effluents between these composites and the control sample of PS/OMT were discussed.

EXPERIMENTAL

Materials

Polystyrene (PS, trade name 158K) and maleic anhydride grafted polystyrene (SMA, trade name SMA-800) were supplied by BASF-YPC Co., and Shanghai Hua Wen Electronic Materials Co., respectively. Sodium benzoate (C_6H_5COONa), ferric nitrate ($Fe(NO_3)_3{\cdot}9H_2O$), hexadecyltrimethylammonium bromide (CTAB), and ethylamine (EA, 65–70%, solution in water) were supplied by Sinopharm Chemical Reagent Co. The organically modified OMT clay (OMT, trade name DK4) was purchased from Zhejiang Fenghong Clay, China, which was a product of Na^+-OMT (MMT, cation exchange capacity 100–120 meq/100 g) modified by dioctadecyl dimethyl ammonium bromide. The α-type ZrP, EA, and CTAB modified α-ZrP (ZrP-EA and ZrP-CTAB), were prepared in our laboratory, details can be found elsewhere.[16,17] All chemicals were used as received without further purification.

Preparation of Iron Oxides Intercalated Layered Compounds

The iron benzoate complex (FePh) was first synthesized by adding 50 mL of 1 mol/L $Fe(NO_3)_3{\cdot}9H_2O$ solution into 125 mL of 0.8 mol/L C_6H_5COONa solution, followed by magnetic stirring of 6 hr at 70°C. The resulted light yellow precipitate was washed with deionized water, collected by centrifugation and dried at 60°C.

To obtain iron oxides intercalated OMT particle (named as Fe-OMT), 4.1 g FePh and 1.0 g OMT were added into 200 mL deionized water then stirred for 8 hr at room temperature. The precipitate was centrifuged, washed and dried at 60°C, the obtained product was refereed as FePh-OMT. Finally, FePh-OMT was calcined at 500°C for 3 hr to yield Fe-OMT particle. The iron oxides intercalated ZrP(CTAB) particle [named as Fe-ZrP(CTAB)] was prepared according to the above method.

For preparation of iron oxides intercalated ZrP(EA) particle [named as Fe-ZrP(EA)], an ZrP exfoliated colloidal dispersion was first prepared by adding 10 mL of 0.4 mol/L EA solution to 150 g of 0.3 wt % ZrP water suspension. Then, 2.0 g FePh was introduced under stirring for 8 hr at room temperature, the precipitate was centrifuged, washed, dried and calcined to obtain Fe-ZrP(EA) particle. All obtained particles were ground and sieved to 300 mesh.

Preparation of PS Composites

PS composites with SMA as compatibilizer (90/10 by weight) containing 10 wt % various additives, were melt compounded using a Brabender mixer at 180°C for 10 min at a screw speed of 90 rpm. The formulations are shown in Table I.

Characterization

The X-ray diffraction (XRD) data were obtained at room temperature using a Rigaku D-Max-Ra rotating anode X-ray diffractometer equipped with a Cu-K_α tube and a Ni filter ($\lambda = 1.5402$ Å). Scanning electron microscopy images were obtained using a Sirion 200 FEG field emission scanning electron microscope (FESEM).

Nitrogen adsorption–desorption measurements were performed at liquid nitrogen temperature (−196°C) on a surface area and porosity analyzer, Tristar II 3020M. Prior to measurements, the un-calcined samples were degassed in vacuum at 50°C for 3 h, while the calcined samples were degassed at 300°C; the data are reproducible to within ±3%.

Thermogravimetric analyses (TGA) were conducted with a TA Q5000 thermoanalyzer instrument. In each case, the 5–10 mg specimens were heated from 30 to 600°C at a heating rate of 20°C/min in a nitrogen or air atmosphere. The TGA data are the average of two measurements. Differential scanning calorimetry (DSC) measurements were performed on a Perkin-Elmer Diamond DSC differential scanning calorimeter. Samples of about 5–10 mg crimp-sealed in aluminum pans were first heated at 10°C/min to 250°C under nitrogen atmosphere and held for 5 min to eliminate previous thermal history before cooling at constant rates of 10°C/min to 0°C. The samples were then heated to 250°C at 10°C/min again and the curves were recorded as a function of temperature.

The ratio of carbon monoxide to carbon dioxide (CO/CO_2) in the combustion effluents from PS composites were evaluated using an apparatus described in the international standard IEC 60754-1,[18] which was equipped with a tube furnace, controlled air supply system and a gas analyzer (Ecom J2KN, Germany). In each case, the 1.0 g specimens were heated at 800°C for 20 min in a stream of dry air (2 L/min), the combustion effluents

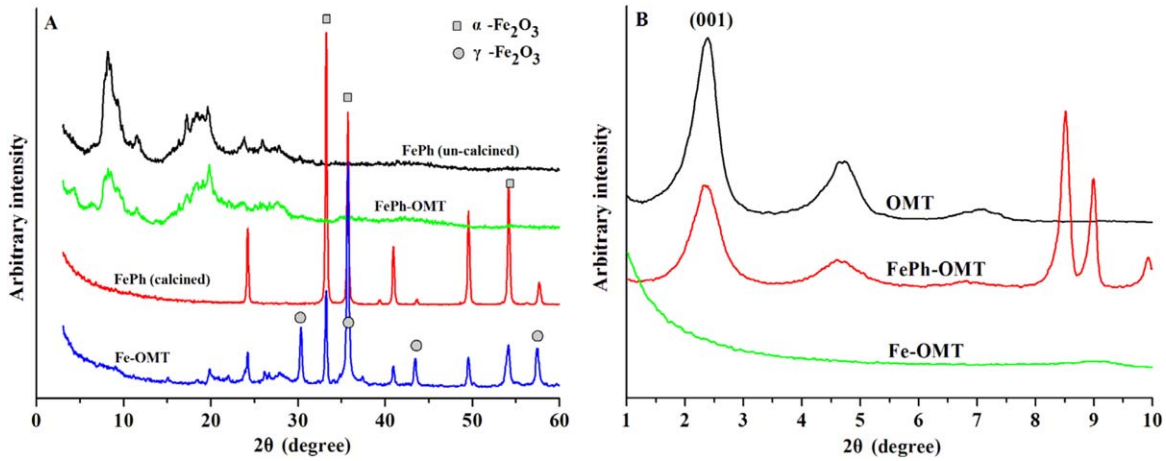

Figure 1. The wide-angle (A) and small-angle (B) XRD patterns of FePh precursor and Fe-OMT particles. [Color figure can be viewed in the online issue, which is available at wileyonlinelibrary.com.]

were collected and the emission of CO and CO_2 were detected by the gas analyzer. The reported data are the average of two measurements.

RESULTS AND DISCUSSION

Characterization of Fe-OMT Particle

Figure 1 shows the XRD patterns of FePh precursor before and after calcinations, FePh-OMT and Fe-OMT. The un-calcined FePh precursor has an ferric hydroxide [FeO(OH)] like structure (JCPDS card No. 22–0353), while α-phase Fe_2O_3 appears in the calcined FePh sample [Figure 1(A)]. Meanwhile, it can be seen that after calcinations, both α-phase Fe_2O_3 with a hematite phase, and γ-phase Fe_2O_3 with a maghemite phase, corresponding well with the JCPDS files (No. 33–0664 and 39–1346, respectively), co-exist in Fe-OMT. Figure 1(B) displays that FePh-OMT has an OMT-like layered structure, but calcinations result in no peaks at lower angle can be found in Fe-OMT, the complete disappearance of the reflection peak may suggest disorder.

The FESEM images of FePh-OMT and Fe-OMT are shown in Figure 2. [Figure 2(A_1)] shows that FePh-OMT particles have an irregular quadrangular prism-like structure with length/width ratio higher than 2. Meanwhile, the stacked clay layers are found to be encapsulated by FePh precursor [Figure 2(A_2)]. After heat treatment, as shown in Figure 2(B_1) and (B_2), a lamellar structure appears in Fe-OMT sample, in which the nanoparticles, mainly α- and γ-phase Fe_2O_3, are bestrewed on clay layers' surfaces or intercalated in clay galleries.

Characterization of Iron Oxides Intercalated ZrP Particles

Figure 3 shows the XRD patterns of Fe-ZrP(CTAB) and Fe-ZrP(EA) particles. Similar to Fe-OMT sample, both α- and γ-phase Fe_2O_3 appear in Fe-ZrP(CTAB) and Fe-ZrP(EA) particles, however, they do not exhibit good crystallization. The magnetic experiments showed that Fe-OMT, Fe-ZrP(CTAB) and Fe-ZrP(EA) particles could be attracted by a magnet, which may confirm the existence of γ-phase Fe_2O_3.

FESEM images in Figure 4 demonstrate that Fe-ZrP(CTAB) has a lamellar microstructure by the stacking of α-ZrP nanoplatelets, with nanoparticles bestrewed on the surfaces. As shown in Figure 5, Fe-ZrP(EA) shows the formation of irregular porous morphology in the micron range (Figure 5A_1); in which the pores are formed by the random stacks of curled ZrP nanoplatelets [Figure 5(A_2)]. However, Fe_2O_3 particles are difficult to be observed on ZrP nanoplatelets, which may suggest that they are embedded.

N_2 Adsorption–desorption Studies

The N_2 adsorption–desorption isotherms of Fe-OMT, Fe-ZrP(CTAB) and Fe-ZrP(EA) particles are shown in Figure 6; the corresponding Brunauer–Emmett–Teller (BET) data are listed in Table II. All the particles exhibit a type-IV isotherm curve according to International Union of Pure and Applied Chemistry (ICPUA) classification.[19] The branch of desorption of the particles shows an inflection knee at relative pressure $P/P_0 = 0.4–0.5$, this kind of hysteresis loop suggests the existence of mesoporous materials with slit-like pores. As listed in Table II, the specific surface area (S_{BET}) and mesoporous volume (V_{meso}) of all particles are higher than those of OMT and ZrP (BET curves did not show here), which may be due to that Fe_2O_3 particles enter into the interlayer spaces of layered compounds keeping the layered structure remained accompanying the elimination of organically surfactants.

Thermal Properties of PS Composites

Thermal degradation and thermo-oxidative degradation of PS composites with Fe-OMT, Fe-ZrP(EA) and Fe-ZrP(CTAB) under a nitrogen and air atmosphere, respectively, were studied and compared with the OMT based PS composite (Figure 7). The data for the temperature at which 5% ($T_{5\%}$) and 50% ($T_{50\%}$) thermal degradation occurs; the temperature at which the maximum mass loss rate occurs (T_{max}) obtained from the derivative TGA curves (DTG); and the fraction of the residue remaining at 500°C, referred to as char, are listed in Table I.

Figure 7(A) shows that the degradation of PS/SMA blend displays a one-step thermal degradation process; stars at 378°C with the maximum mass loss rate at 372°C, leaving 0.7% residue at 500°C. The control sample of PS/SMA/OMT exhibits higher thermal stability with increasing temperature compared

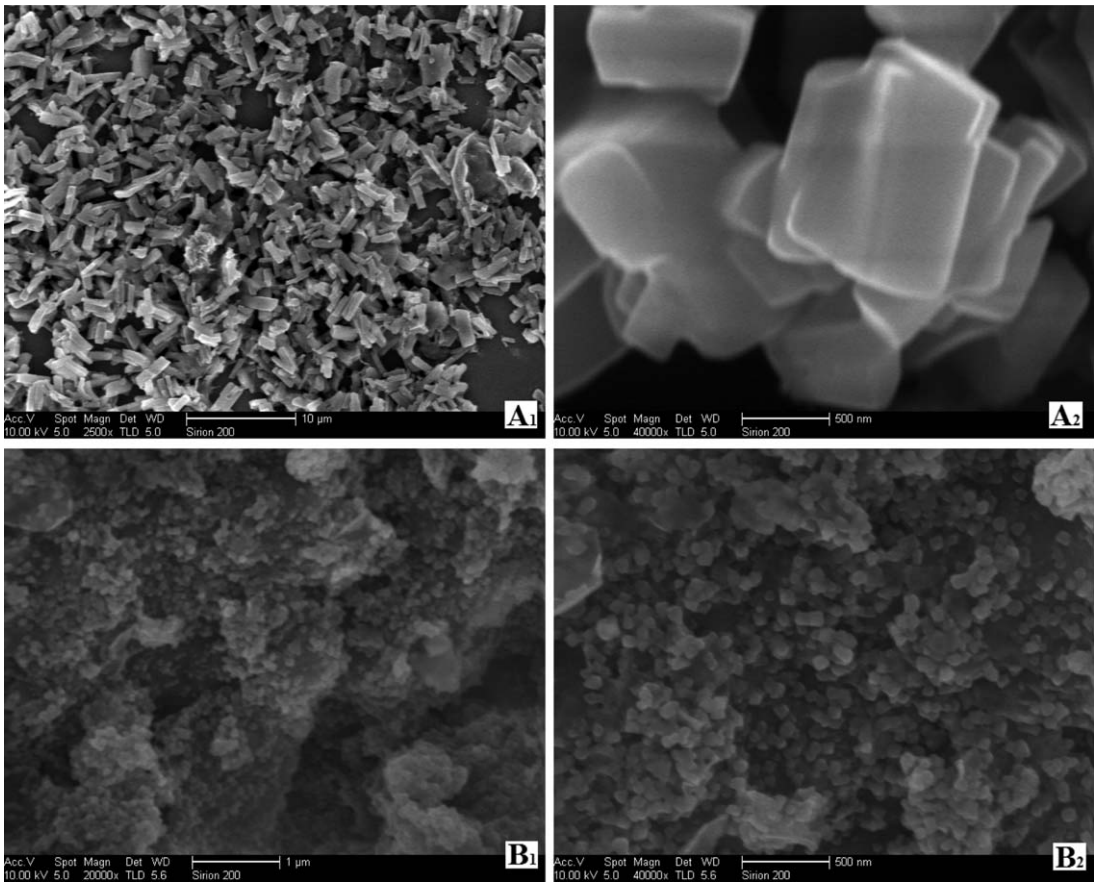

Figure 2. SEM images of samples (A_1 and A_2) FePh-OMT, and (B_1 and B_2) Fe-OMT at different magnifications.

with PS/SMA, but earlier initial weight loss at 370°C due to the lower onset temperature of OMT. For the composites containing Fe-OMT, Fe-ZrP(EA) and Fe-ZrP(CTAB), they exhibit enhanced $T_{5\%}$ and leave about 10–11% char yields greater than that of 6.3% for PS/SMA/OMT. However, the obtained char residues are almost equal to the calculated values; that is 10% from the particles and 0.7% from PS/SMA, which means that the presence of anyone of the particles does not accelerate the formation of the char yields additionally. The reason is possibly due to that these Fe_2O_3 intercalated OMT and ZrP particles can not form an efficient protective surface barrier as the nanodispersed layers of OMT and ZrP in polymer nanocomposites do.

Thermo-oxidation stability of PS/SMA with OMT, Fe-OMT, Fe-ZrP(EA) and Fe-ZrP(CTAB) in an air atmosphere is shown in Figure 7(B). It can be seen that all samples show a one-step thermo-oxidation degradation and exhibit higher stability compared with PS/SMA blend. Meanwhile, PS/SMA/OMT sample shows the highest stability among these samples below 430°C,

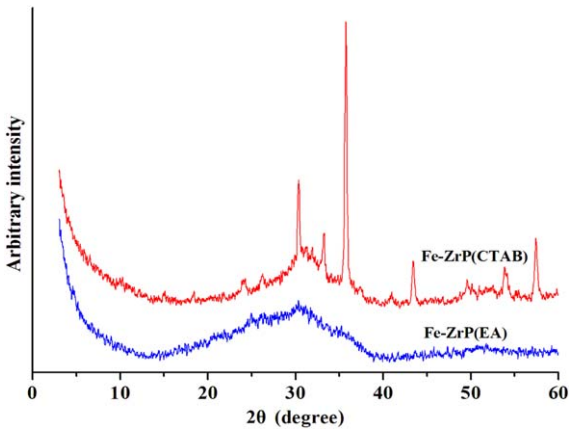

Figure 3. XRD patterns of Fe-ZrP(CTAB) and Fe-ZrP(EA) particles. [Color figure can be viewed in the online issue, which is available at wileyonlinelibrary.com.]

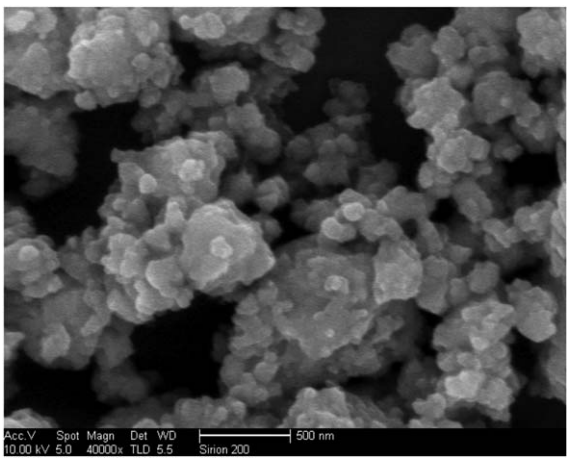

Figure 4. SEM images of Fe-ZrP(CTAB).

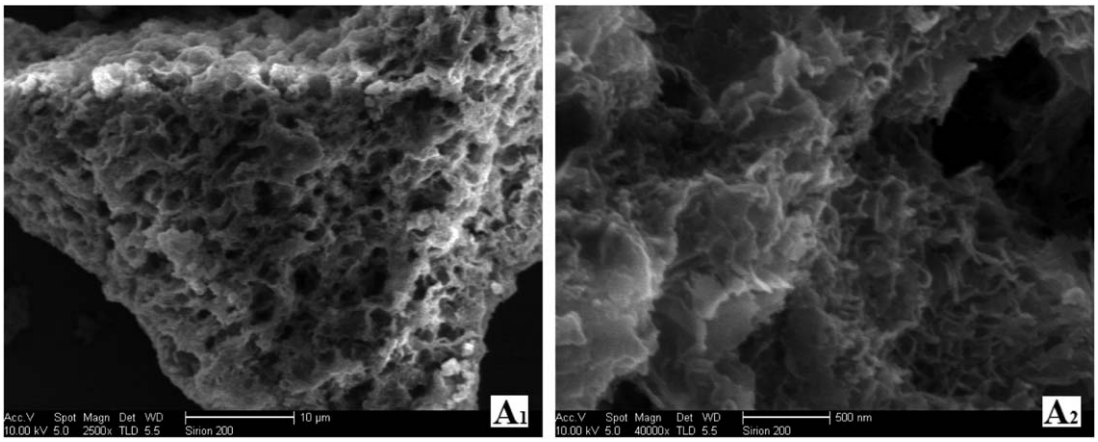

Figure 5. SEM images of Fe-ZrP(EA) at different magnifications.

which is due to that the nano-dispersed clay layers prevent the mass and heat transfer more efficient than those porous particles. Similar to thermal degradation observations, PS/SMA/Fe-OMT, PS/SMA/Fe-ZrP(EA) and PS/SMA/Fe-ZrP(CTAB) do not leave more char residues than the calculated.

Figure 8 shows the DSC thermograms of PS/SMA blend and its composites; their corresponding glass transition temperature (T_g) data are summarized in Table I. As expected, T_g of PS composites is increased with the incorporation of OMT, Fe-OMT, Fe-ZrP(EA) and Fe-ZrP(CTAB) particles. Meanwhile, PS/SMA/Fe-OMT, PS/SMA/Fe-ZrP(EA) and PS/SMA/Fe-ZrP(CTAB) composites show a higher value of T_g compared with PS/SMA/OMT, which suggests the interactions between polymeric matrix and Fe-OMT, Fe-ZrP(EA) and Fe-ZrP(CTAB) are more stronger; the improved adhesion therefore restricts the segmental motion near the organic–inorganic interface efficiently.

CO/CO_2 Ratio

The change of CO/CO_2 ratio in combustion effluents can reflect the extent of oxidation of the polymeric materials. The influence of OMT, Fe-OMT, Fe-Zr(EA) and Fe-Zr(CTAB) on CO/CO_2

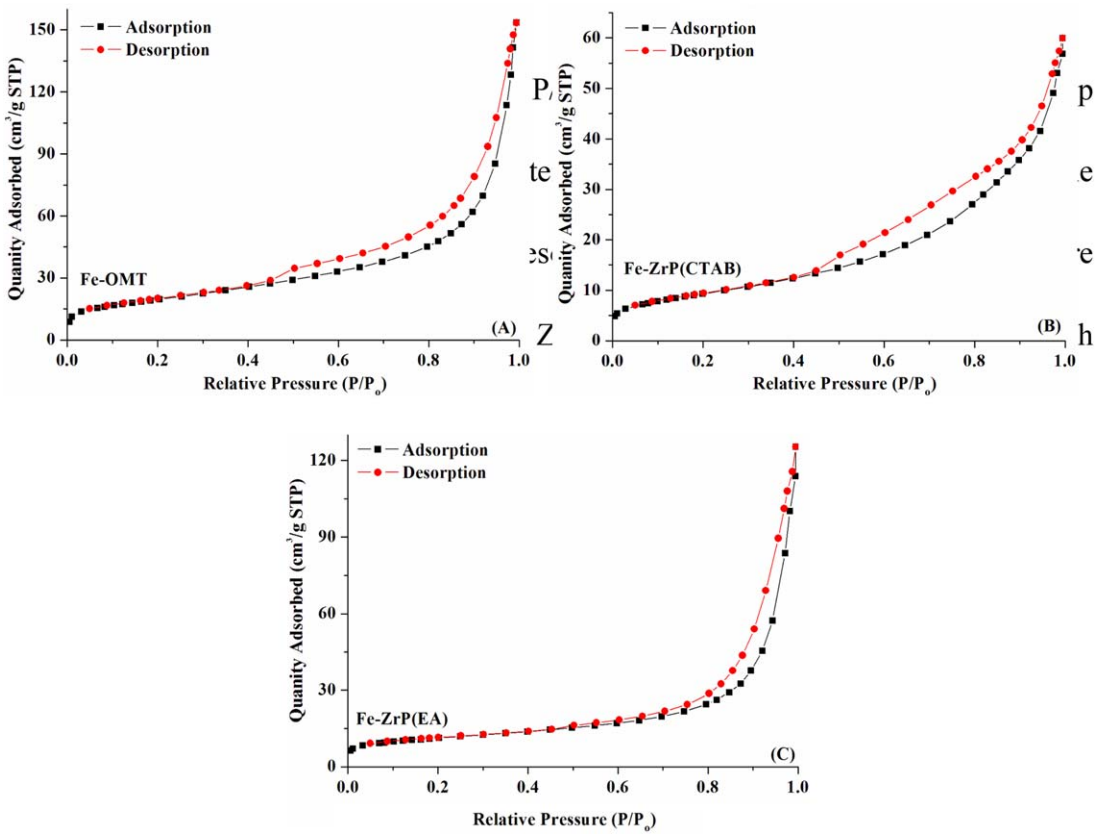

Figure 6. Nitrogen adsorption–desorption isotherm linear plots for (A) Fe-OMT, (B) Fe-ZrP(CTAB), and (C) Fe-ZrP(EA) particles. [Color figure can be viewed in the online issue, which is available at wileyonlinelibrary.com.]

Table II. BET Properties of Fe-OMT, Fe-ZrP(CTAB), and Fe-ZrP(EA) Particles

Samples	S_{BET} (m^2/g)	V_{meso}[a] (cm^3/g)	Average pore diameter[a] (nm)
Fe-OMT	70.5	0.24	13.2
Fe-ZrP(CTAB)	33.6	0.09	9.2
Fe-ZrP(EA)	40.0	0.18	19.7
MMT	7.3	0.04	28.5
α-ZrP	3.9	0.02	47.4

S_{BET}, specific surface area; V_{meso}, mesoporous volume.
[a] Calculated from BJH method (adsorption).

ratio in the combustion effluents from PS composites are listed in Table I. The incorporation of anyone of the particles leads PS composites to exhibit higher ratio in comparison with PS/SMA counterpart, which suggests that the extent of incomplete oxidation increases.

PS is commonly supposed not to undergo charring at microscale fire testing, but Clark has reported that a superficial layer of carbon can be formed on the surface when PS is ignited.[13] As far as we know, the carbon plays an important effect in the combustion of polymers; and the flame retardant effect from carbon is related to the oxidation reactions as followings:

$$C+1/2O_2 \rightarrow CO+110.5\,kJ/mol \quad (1)$$

$$CO+1/2O_2 \rightarrow CO_2+284.1\,kJ/mol \quad (2)$$

$$C+O_2 \rightarrow CO_2+394.2\,kJ/mol \quad (3)$$

It is apparently that the heat released from reaction (3) is almost four times higher than that from reaction (1). The result in formation of CO process is therefore conducive to attenuating the complete oxidative of carbon (reactions 2 and 3) then reducing the heat released, which is of benefit to reduce the thermal energy supply for volatilization by the condensed phase oxidation and stop burning. The increased CO/CO_2 ratios from the composites may be due to that during the charring formation process, the reaction activation centers of carbon are occupied by the powders, particularly those particles of layered compounds intercalated with Fe_2O_3 have higher specific surface area and mesoporous volume, which prevents carbon to be oxidized deeply.

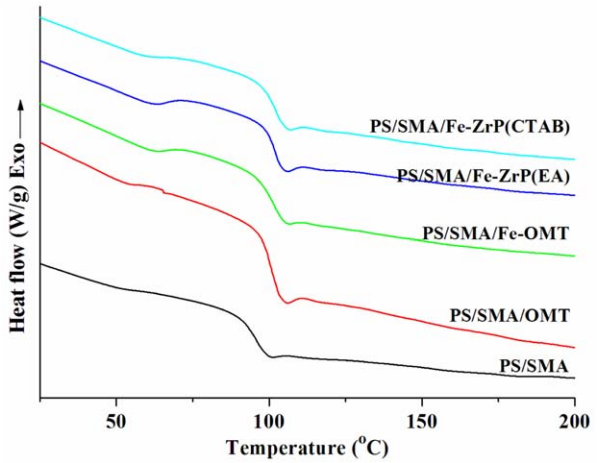

Figure 8. DSC thermograms of PS/SMA blend and its composites with various particles. [Color figure can be viewed in the online issue, which is available at wileyonlinelibrary.com.]

It is also noted that the composites of PS/SMA/Fe-Zr(EA) and PS/SMA/Fe-ZrP(CTAB) exhibit a higher CO/CO_2 ratio compared with either PS/SMA/OMT or PS/SMA/Fe-OMT. The possible reason may be that the introducing of iron oxides further increases the acidity of α-ZrP that has been taken as a solid acid, which is helpful for polymeric matrix dehydration and carbonization, and prevents the complete oxidation of carbon to release a large amount of heat. That is similar to the flame retardant mechanism of phosphorus-containing flame retardants such as red phosphorous (RP), which always increases the production of CO from the burning of polymeric materials.[20]

CONCLUSIONS

The particles of OMT and ZrP intercalated with both α- and γ-phase Fe_2O_3 having mesoporous lamellar structure were

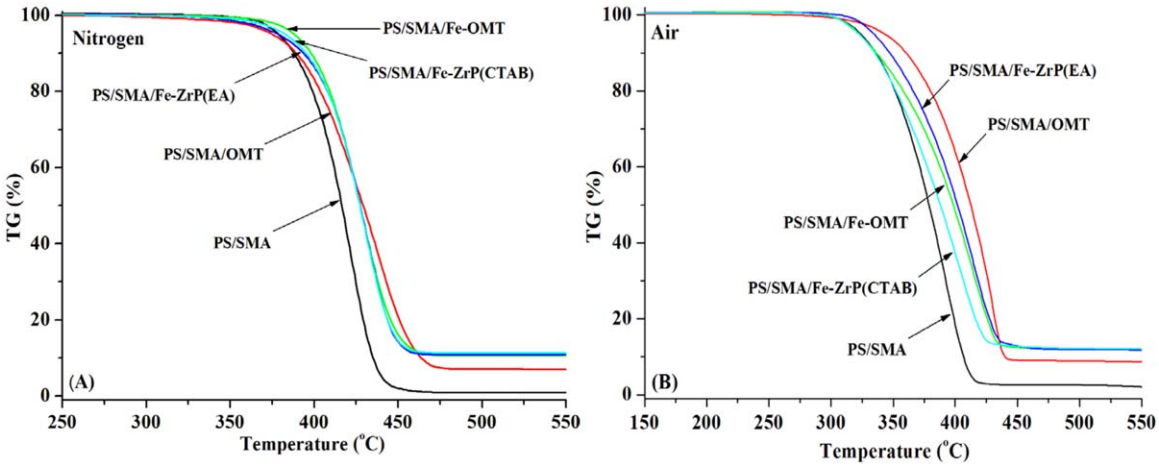

Figure 7. TGA curves of PS composites with 10 wt % various additives under a nitrogen and air atmosphere. [Color figure can be viewed in the online issue, which is available at wileyonlinelibrary.com.]

synthesized. The presence of Fe-OMT, Fe-ZrP(EA), and Fe-ZrP(CTAB) led PS/SMA composites to exhibit an increased thermal degradation onset temperature compared with PS/SMA/OMT composite; but the later showed the highest thermo-oxidative stability among those composites. Unexpected, the introducing of iron oxides to layered compounds did not promote the complete combustion of PS composites to reduce the emission of CO. It seems that the incorporations of Fe-OMT, Fe-ZrP(EA) and Fe-ZrP(CTAB) into PS help to stop burning by reducing the thermal energy supply for volatilization; however, the emission of toxic non-irritating gas, CO, will cause serious non-thermal hazard during combustion.

ACKNOWLEDGMENTS

The work was financially supported by National Natural Science Foundation of China (No. 51276054 and 51403048), Program for Excellent Young Talents in University of Anhui Province, National Undergraduate Innovation and Entrepreneurship Training Programs (No. 201311059005 and 201311059006), and Deutscher Akademischer Austausch Dienst (DAAD).

REFERENCES

1. Liu, J. C.; Fu, M. Y.; Jing, M. M.; Li, Q. Y. *Polym. Adv. Technol.* **2013**, *24*, 273.
2. Arora, A.; Choudhary, V.; Sharma, D. K. *J. Polym. Res.* **2011**, *18*, 843.
3. Tsai, T. Y.; Lin, M. J.; Chuang, Y. C.; Chou, P. C. *Mater. Chem. Phys.* **2013**, *138*, 230.
4. Dominkovics, Z.; Jozsef, H.; Fekete, E.; Pukanszky, B. *Polym. Degrad. Stab.* **2011**, *96*, 581.
5. Cai, G. P.; Wilkie, C. A. *J. Fire Sci.* **2014**, *32*, 35.
6. Yang, D. D.; Hu, Y.; Xu, H. P.; Zhu, L. P. *J. Appl. Polym. Sci.* **2013**, *130*, 3038.
7. Gupta, M. C.; Viswanath, S. G. *J. Therm. Anal. Calorim.* **1998**, *53*, 931.
8. El-Brolossy, T. A.; Ibrahim, S. S. *Thermochim. Acta* **2010**, *509*, 46.
9. Wu, N.; Yang, R. J. *Polym. Adv. Technol.* **2011**, *22*, 495.
10. Laachachi, A.; Cochez, M.; Ferriol, M.; Lopez-Cuesta, J. M.; Leroy, E. *Mater. Lett.* **2005**, *59*, 36.
11. Laachachi, A.; Leroy, E.; Cochez, M.; Ferriol, M.; Lopez-Cuesta, J. M. *Polym. Degrad. Stab.* **2005**, *89*, 344.
12. Tiwary, P.; Guria, C. *J. Polym. Environ.* **2010**, *18*, 298.
13. Martel, B. *J. Appl. Polym. Sci.* **1988**, *35*, 1213.
14. Gandía, L. M.; Vicente, M. A.; Gil, A. *Appl. Catal. B: Environ.* **2002**, *38*, 295.
15. Chen, M.; Fan, L. P.; Qi, L. Y.; Luo, X. Y.; Zhou, R. X.; Zheng, X. M. T. *Catal. Commun.* **2009**, *10*, 838.
16. Lu, H. D.; Wilkie, C. A.; Ding, M.; Song, L. *Polym. Degrad. Stab.* **2011**, *96*, 885.
17. Lu, H. D.; Wilkie, C. A. *Polym. Degrad. Stab.* **2010**, *95*, 2388.
18. International Standard, IEC 60754-2, Test on gases evolved during combustion of materials from cables-Part 1: Determination of the halogen acid gas content, 2011-11, Edition 3.0.
19. Li, B. S.; Liu, Z. X.; Han, C. Y.; Liu, J. J.; Zuo, S. L.; Zhou, Z. Y.; Pan, X. M. *J. Mol. Catal. A-Chem.* **2011**, *348*, 106.
20. Braun, U.; Schartel, B. *Macromol. Chem. Phys.* **2004**, *205*, 2185.